




Original Article

# A Dynamic Optimization Approach for Solving Spine Kinematics While Calibrating Subject-Specific Mechanical Properties

WEI WANG <sup>1,2,3</sup>, DONGMEI WANG,<sup>1</sup> ANTOINE FALISSE,<sup>2</sup> PIETER SEVERIJNS,<sup>4</sup>  
THOMAS OVERBERGH,<sup>4</sup> LIEVEN MOKE,<sup>4</sup> LENNART SCHEYS,<sup>4</sup>  
FRIEDL DE GROOTE,<sup>2</sup> and ILSE JONKERS<sup>2</sup>

<sup>1</sup>School of Mechanical Engineering, Shanghai Jiao Tong University, Shanghai, China; <sup>2</sup>Department of Movement Sciences, KU Leuven, Leuven, Belgium; <sup>3</sup>The CAS Key Laboratory of Human-Machine Intelligence-Synergy Systems, Shenzhen Institute of Advanced Technology (SIAT), Chinese Academy of Sciences, Shenzhen, China; and <sup>4</sup>Department of Development and Regeneration, Institute for Orthopaedic Research and Training, KU Leuven, Leuven, Belgium

(Received 18 February 2020; accepted 31 March 2021; published online 13 April 2021)

Associate Editor Elena S. Di Martino oversaw the review of this article.

**Abstract**—This study aims to propose a new optimization framework for solving spine kinematics based on skin-mounted markers and estimate subject-specific mechanical properties of the intervertebral joints. The approach enforces dynamic consistency in the entire skeletal system over the entire time-trajectory while personalizing spinal stiffness. 3D reflective markers mounted on ten vertebrae during spine motions were measured in ten healthy volunteers. Biplanar X-rays were taken during neutral stance of the subjects wearing the markers. Calculated spine kinematics were compared to those calculated using inverse kinematics (IK) and IK with imposed generic kinematic constraints. Calculated spine kinematics compared well with standing X-rays, with average root mean square differences of the vertebral body center positions below 10.1 mm and below 3.38° for joint orientation angles. For flexion/extension and lateral bending, the lumbar rotation distribution patterns, as well as the ranges of rotations matched *in vivo* literature data. The approach outperforms state-of-art IK and IK with constraints methods. Calculated ratios reflect reduced spinal stiffness in low-resistance zone and increased stiffness in high-resistance zone. The patterns of calibrated stiffness were consistent with previously reported experimentally determined patterns. This approach will further our insight into spinal mechanics by increasing the physiological representativeness of spinal motion simulations.

**Keywords**—Force-dependent optimization, Kinematics redundancy, Parameter estimation, Spinal stiffness, Spine.

## INTRODUCTION

Evaluating human movement kinematics is essential in biomechanical analysis. Joint kinematics are also a primary input for most kinematics-driven models to compute joint loading and muscle forces.<sup>6</sup> However, although dedicated musculoskeletal models of the spine have been developed (e.g., Ref. 2), such analyses have only been used to a limited extent to analyze spine loading during movement. This is due to difficulties to measure accurate intervertebral motions caused by many degrees-of-freedom (DoF) of the spine as well as the relatively small motion of individual vertebrae.

Different approaches have been used to estimate spinal kinematics as accurately as possible. Medical imaging approaches are often regarded as gold standard as they can provide detailed geometric information. However, most imaging approaches are either limited by two-dimensional information (e.g., static X-rays and dynamic fluoroscopy<sup>1</sup>) or by restricted postures (e.g., CT, biplanar fluoroscopy and MRI), failing to capture three-dimensional (3D) dynamic motions (e.g., gait). Therefore, motion capture techniques combined with marker-based inverse kinematics (IK) are commonly used for estimating motions as these are non-invasive, flexible, and minimally interfering with activities of daily living. The IK method estimates the pose of the spine by minimizing the error between modeled marker positions based on a kinematic model and measured marker positions at each time frame (least square minimization). Given the high kinematic

Address correspondence to Dongmei Wang, School of Mechanical Engineering, Shanghai Jiao Tong University, Shanghai, China. Electronic mail: dmwang@sjtu.edu.cn

redundancy in the spine, accurate estimation of intervertebral joint kinematics is very challenging; space constraints on the spine prevent placement of sufficient reflective markers on the spine to capture all DoFs of the intervertebral joints. Skin artefacts during dynamic motions make it even harder to track the often small intervertebral joint displacements.<sup>30</sup> Therefore, to reduce the number of DoFs, constraints imposing constant ratios between lumbar kinematic variables have been suggested. In such approaches, the estimated intervertebral joint rotations are proportional to the overall lumbar rotations and coupled to another (IK + constraints), and translational DoFs are typically locked.<sup>3</sup> However, these constraints represent an oversimplification as it is known from imaging studies that the distribution of total lumbar rotations over the different vertebral levels is motion-dependent as it changes with trunk rotation, lumbar posture, and loading.<sup>1,23</sup>

IK methods only account for kinematic constraints, whereas optimization-based methods enable imposing additional dynamic constraints.<sup>23</sup> Marra *et al.*<sup>14</sup> proposed an approach called force-dependent kinematics to improve the estimation of secondary knee kinematics, i.e. the DoFs with a small ROM (e.g., knee translations). Secondary kinematics are iteratively updated until quasi-static force equilibrium between contact, muscle and ligament forces is reached. However, this method is not applicable for estimating both rotational and translational spine kinematics as both of them need to be determined.<sup>10</sup> Shojaei *et al.*<sup>23</sup> proposed an alternative optimization approach where the lumbar rotations are updated by minimizing the sum of squared lumbar muscle stresses, while neglecting lumbar translations. However, the rotations are calculated based on a heuristic procedure that relies on multiple local optimization problems that each accounts for inverse skeleton dynamics and muscle force equilibrium for each spinal level independently. This approach does not guarantee dynamic consistency in the entire skeletal system. Another drawback of both above-described methods,<sup>14,23</sup> as well as of most other optimization studies on spine kinematics (e.g., Ref. 10), is that they only account for static force equilibrium and thus estimate kinematics at each time frame independently. As a result, there is no dynamic consistency over the entire time trajectory which will influence kinetic analysis as it has been demonstrated that kinetic predictions and load-related calculations are sensitive to errors in static kinematic measurements.<sup>6</sup> Finally, in previous studies (e.g., Refs. 10 and

23), the input information on bone positions for solving spine kinematics commonly originated from static medical images, therefore restricting evaluation of dynamic motion compared to marker-based measurements. To our knowledge, no studies analyzed the effect of accounting for dynamic consistency throughout the entire spine motion neither through marker-based nor medical imaging-based kinematic analysis.

None of the above-described methods for estimating spine kinematics account for the mechanical properties of the intervertebral joint, which play an important role in constraining spine motion. Given the high stiffness of the intervertebral joints, their mechanical properties largely determine joint kinematics.<sup>14</sup> Moreover, these mechanical properties are highly subject-specific. In our previous work,<sup>26</sup> we already implemented physiological functional spinal units with comprehensive nonlinear stiffness properties into a rigid-body model of the full thoracolumbar spine, containing different parameter sets that account for differences in *in vitro* specimens. However, preknowledge of physiological conditions are not always available, thereby preventing a proper selection of stiffness parameter set. Petit *et al.*<sup>20</sup> developed a method to calibrate stiffness properties. In their approach, the model's mechanical properties are adjusted to minimize the difference between simulated and measured spinal curvature angles during maximal voluntary lateral bending. However, this approach does not account for the dynamic properties of the movement and the high nonlinearity of intervertebral stiffness. Furthermore, stiffness calibration was limited to three sets of generic stiffness for all seventeen levels of the spine between T1 and L5. To appropriately account for the influence of spine stiffness on intervertebral movement, there is a need for calibrated stiffness properties for each individual intervertebral DoF.

This study proposes a dynamic optimization approach to estimate spine kinematics from trajectories of skin-mounted markers while simultaneously calibrating spine stiffness by enforcing the dynamic consistency of the movement. As such, this study aims to improve the accuracy of estimates of dynamic spine motion based on 3D motion capture data by imposing dynamic equilibrium over the entire skeletal system and the entire movement cycle. The estimated spinal kinematics were evaluated against kinematic estimations obtained from state-of-the-art IK methods, with and without generic kinematic constraints as well as standing bi-planar radiographs (gold truth) and published *in vivo* reference values.

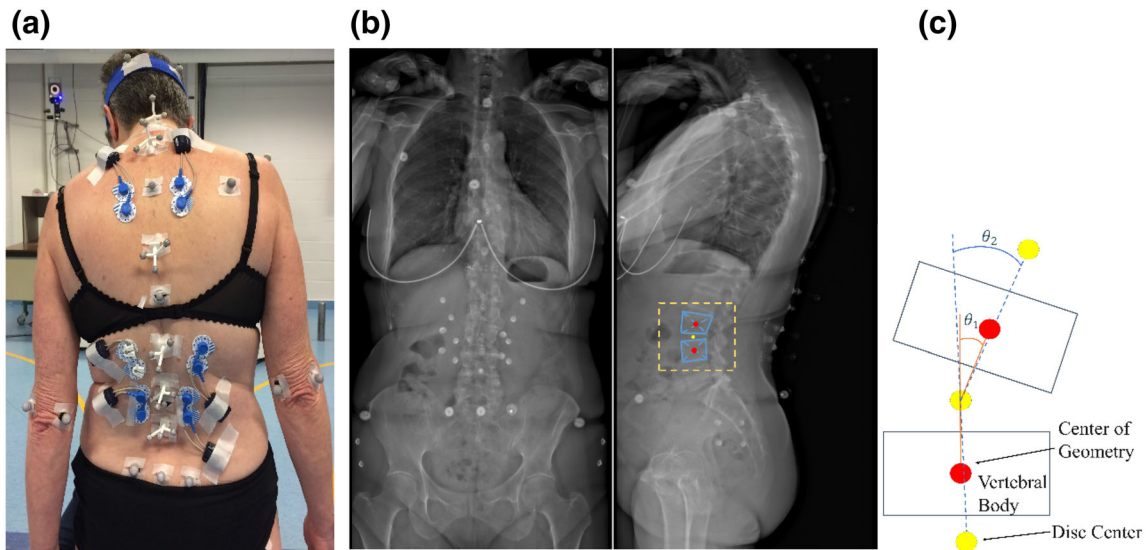


**FIGURE 1.** Illustrations of (a) the marker placement protocol on the spine, (b) the coronal and sagittal images measured by the Bi-planar X-rays system, and (c) the methods used to calculate sagittal joint orientation angles on X-rays. Two approaches were used to estimate the joint orientation. First, we determined the angles between the lines (being projected on sagittal plane) connecting the disc centers, which we manually indicated on the X-ray images. Second, we determined the angles between the lines connecting the center of geometry of the vertebral bodies and the corresponding disc center on X-ray. The results of both methods were averaged to reduce measurement errors.

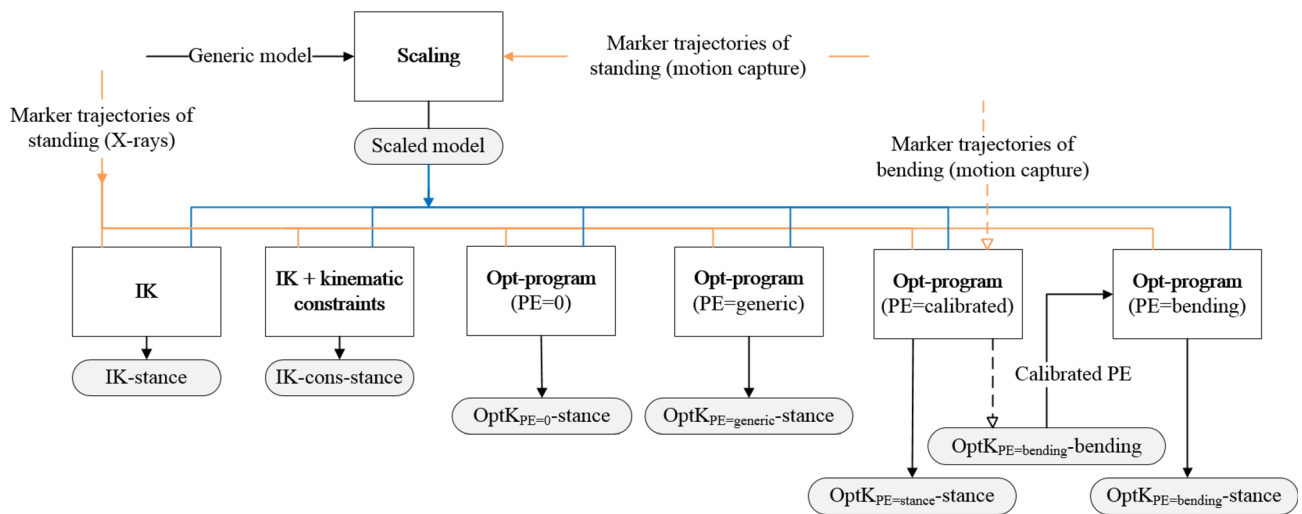


**FIGURE 2.** A schematic showing different kinematic approaches of stance based on marker positions. IK- refers to kinematic solutions using Inverse Kinematics tool in OpenSim, and IK-cons- refers to IK solutions with kinematic constraints; OptK- refers to kinematic solutions using the proposed dynamic optimization program (Opt-program) where the forces of passive element (PE) generated by spinal stiffness are taken into account. PE=0 indicates that the PE does not generate forces, PE=generic indicates the generic values developed by Wang *et al.*<sup>26</sup> are used and not calibrated, PE = calibrated indicates the parameters are simultaneously calibrated while optimizing the current motion, PE = bending indicates the parameters are obtained from optimizing the other bending motions that include spine flexion/extension (F/E), lateral bending (LB) and a combined motion containing full ranges of both F/E and LB. Note that to compare the simulated spine alignment with X-ray data, we used extracted marker positions of stance on X-rays (Fig. 1b)<sup>18</sup> as input motion for the above mentioned approaches to estimate spine kinematics (due to no optical motion capture system on when we took the X-rays), so the comparisons were based on the same posture.

## MATERIALS AND METHODS

### Measurements

Spinal motions of ten healthy subjects (three males, seven females) were measured by an optical tracking system (VICON, UK). The mean (standard deviation (SD)) age, height and weight of the subjects were 67.85 (6.95) years, 1641.4 (73.4) mm and 60.37 (15.45) kg respectively. Measured motions included (1) static neutral upright stance, (2) full range of spine flexion/extension ( $F/E$ ) while seated, with hands crossed over the back of head to keep an upright upper trunk, and (3) full range of lateral bending (LB, from neutral to maximal left bending then to maximal right bending) while seated, with hands hanging on either side. Retroreflective markers (see Fig. 1a) were positioned on the processus spinosus of the vertebrae (six asymmetrical three-marker-clusters<sup>27</sup> on T1, T3, T7, T11, L2 and L4; four single markers on T5, T9, T12, and L3; one cluster weights around 5–8 g), left/right anterior/posterior superior iliac spine, and sacrum.<sup>17,18,22</sup> Bi-planar X-rays (EOS Imaging, France) were also taken during neutral upright stance of the subjects wearing markers (Fig. 1b) and used as gold truth. This study was approved by the institutional review board of UZ Leuven. All participants signed a written informed consent before the start of the experiment.

### Data Processing

We used an existing musculoskeletal model (OpenSim, version 4.0) of a fully articulated thoracolumbar spine<sup>2</sup> to process the collected experimental data. All 6-DoF of the intervertebral joints spanning from T1 to S1 were enabled, allowing three rotations and three translations in each joint. Based on our previous work,<sup>26</sup> we incorporated OpenSim ExpressionBasedBushingForce elements into the model to account for the stiffness originating from passive structures. Each bushing element (hereafter referred to as passive element (PE)) generates force as a function of the relative displacement of the two bushing frames connected to the articulating bodies. We used OpenSim's Scale tool to scale the generic model, non-pathologic male adult (25 years, 1750 mm, 78 kg), to the subjects' anthropometry.

The scaled model together with the measured 3D marker trajectories of motions were used to calculate the IK solution through running OpenSim's Inverse Kinematics tool (Fig. 2). In addition, we also generated IK solutions while imposing linear kinematic constraints describing the relation between intervertebral displacements in different joints (hereafter referred to as 'IK-cons'). The constraints imposed

constant interpolation ratios for  $F/E$ , LB, and axial rotation (AR) individually at the different levels. The ratios were based on the reported values in literature: IK-cons1 refers to Christophy *et al.*<sup>3</sup> (for lumbar  $F/E$ , LB, and AR), IK-cons2 refers to Bruno *et al.*<sup>2</sup> (for thoracic and lumbar  $F/E$ , LB, and AR), IK-cons3 refers to Shojaei *et al.*<sup>23</sup> (for lumbar  $F/E$ ). Detailed ratios are listed in the Supplementary table. Preliminary data analysis indicated that IK solutions with 6-DoF enabled for each intervertebral joint yielded unrealistic vertebral positions, as expected due to the excessive kinematic redundancy. Therefore, these results were excluded from further analysis and only IK and IK-cons solutions generated using a model with three-rotational DoF for each intervertebral joint (the common condition in most studies) were further analyzed.

Alternatively, we estimated spine kinematics by solving a dynamic optimization program (referred to as 'Opt-program'). We solved for joint kinematics (positions and velocities of generalized coordinates) and stiffness parameters that minimized the difference between the modeled and measured marker trajectories as well as the intersegmental forces while satisfying skeletal dynamics. The objective function  $J$  in (1) is the weighted sum of a data-tracking term and a term penalizing large generalized active joint segmental forces (forces and moments):

$$J = \int_{t_0}^{t_f} w_1 p(q) - \hat{p}^2 + w_2 F_{\text{Act}}^2(q, \dot{q}, \ddot{q}) dt, \quad (1)$$

where  $t$  is time,  $t_0$  and  $t_f$  are the start and end time of the movement,  $q$  and  $\dot{q}$  are positions and velocities of the model's generalized joint coordinates,  $\ddot{q}$  are joint accelerations,  $p$  and  $\hat{p}$  are simulated and measured marker coordinates, respectively, where  $p$  are rigidly linked to the mounted body and thereby  $p$  is as a function of the coordinate positions  $q$ ,  $F_{\text{Act}}$  is the vector containing active joint segmental forces (in all 6-DoF) from T1 to sacrum,  $w_1 = 1000$  and  $w_2 = 10$  are weight factors determined heuristically to make the two cost terms of similar magnitude. The first tracking term ( $p - \hat{p}^2$ ) minimizes the differences between the measured ( $\hat{p}$ ) and simulated ( $p$ ) marker positions. The second term ( $F_{\text{Act}}^2$ ) minimizes the sum of squared generalized active joint segmental forces from T1 to sacrum, which are produced by muscles, and thus minimizes the muscle effort being used. This objective function was minimized subject to bounds and constraints. Upper and lower bounds for  $q$  were based on reported maximum RoM values in Refs. 21 and 29 that were increased by 150%. Maximum deviation for  $p$  was set to 40 mm. Dynamic constraints impose that joint kinematics  $q$  and  $\dot{q}$  should be consistent with skeletal dynamics:

$$M(q)\ddot{q} + G(q) + C(q, \dot{q}) + F_{\text{Act}}(q, \dot{q}, \ddot{q}) + F_{\text{PE}}(q, p) = 0, \quad (2)$$

where  $M(q)$  is the system mass matrix,  $G(q)$  is the vector of gravitational forces,  $C(q, \dot{q})$  is the vector of Coriolis and centrifugal forces, and  $F_{\text{PE}}$  is the vector containing the corresponding passive forces generated by joint stiffness in response to joint displacement:

$$F_{\text{PE}_i}(q_i) = A_i(e^{B_i q_i} - 1), \quad (3)$$

where vector  $A$  and  $B$  are static optimization variables (time-independent parameters) that were introduced as the coefficients of the nonlinear passive element,  $i$  indicates the vertebral level. The initial values of  $A$  and  $B$  were generic parameters based on fitting *in vitro* loading displacement of spinal intervertebral joints (for details, see our previous work<sup>26</sup>).

We used direct collocation method<sup>4</sup> to solve this dynamic optimization problem. Software Matlab and open-source software CasADi were used to formulate this nonlinear optimal control problem.<sup>8</sup> Computation of skeletal inverse dynamics and the virtual marker positions were obtained through the OpenSim libraries. Finally, this nonlinear program is solved using IPOPT solver (Interior Point Optimizer). All computations were performed on an Intel Core i7-6560U 2.21 GHz processor with 16 GB RAM.

#### *Evaluation of the Kinematic Results and Calibrated Stiffness*

We first assessed the estimated spine alignment in upright neutral stance, i.e., the body positions and orientations of vertebral bodies based on measured 3D marker positions. Figure 2 gives an overview of the six different approaches we used to estimate joint kinematics during standing. We applied the inverse kinematic approach (IK) and the inverse kinematic approach with kinematic constraints (IK-cons), as well as the dynamic optimization approach described above (resulting kinematic solutions are referred to as ‘OptK’). More specific, we compared OptK solutions where the stiffness parameters were simultaneously calibrated while optimizing the current motion (OptK<sub>PE</sub> = calibrated), OptK solutions with predefined stiffness parameters, which were either the generic parameters (OptK<sub>PE</sub> = generic<sup>26</sup>) or parameters obtained from optimizing spine (*F/E*) motion (OptK<sub>PE</sub> = *F/E*), LB motions (OptK<sub>PE</sub> = LB), and a combined motion containing *F/E* and LB (OptK<sub>PE</sub> = *F/E* + LB). We analyzed these different options as we assumed that the combined *F/E* and LB motion would contain more information resulting in more valid (i.e., representative of the subjects) parameter estimates.<sup>7</sup> In

addition, we performed OptK without any forces generated by the PE (i.e., OptK<sub>PE</sub> = 0) to evaluate the effect between solely accounting for dynamic consistency and accounting for both dynamic consistency as well as passive contributions from PE. It should be noted that we used marker positions of stance from optical motion capture to scale the generic model, and marker trajectories of all bending motions were also from optical motion capture system.

Marker-based estimates of spine alignment were compared to spine alignments derived from X-rays, which is considered as the gold standard data source. The alignment curve was evaluated in terms of the 3D position of the centers of geometry (CoG) of the vertebrae bodies and sagittal joint orientations. We obtained the CoG by manually identifying the approximate center of vertebral bodies on X-rays. We determined joint orientation as the relative joint orientations between adjacent vertebrae on the sagittal plane (Fig. 1(c)). The alignment curve was derived from the marker-based kinematic estimates by connecting the midpoint between every two joint centers (approximated centers of discs) in the estimated pose of the model. We assessed the mean absolute error between marker-based and X-ray-based CoG positions (from T1 to L5) and joint orientations (from T7-T8 to L4-L5) across the ten subjects.

Additionally, we evaluated the kinematics distribution pattern for the different kinematic estimates based on motion sharing ratios (MSR),<sup>1</sup> i.e., a ratio of the joint angle of each lumbar intervertebral joint with respect to the motion of the entire lumbar spine at each time instant during motions. As initial and final postures were close to upright corresponding to zero joint angles in our model, we excluded the first and last 20th percent of the motion cycle from the analysis to avoid error due to dividing joint motions by small total rotations.<sup>1</sup> The coefficient of multiple correlation (CMC)<sup>27</sup> was calculated to evaluate the similarity in MSR ratio between all subjects. The average MSR of *F/E* and LB of all subjects were compared to the published *in vivo* data derived from medical-imaging or bone pine data during dynamic *F/E* and LB.<sup>5,19,21,25</sup> In addition, the range of intervertebral joint rotation during *F/E* and LB calculated using all six approaches were compared to *in vivo* reference data for *F/E*<sup>9,25</sup> (similar seated maximal *F/E*) and LB<sup>5,12,19,21</sup> in literature.

We evaluated the calibrated PE parameters by comparing the calibrated stiffness values to a range of generic stiffness values modeled based on published data of healthy subjects of mean age around 50 years old<sup>26</sup> and previously reported stiffness patterns in subjects with similar age as our test subjects. Due to the high nonlinearity of the functional spinal units,

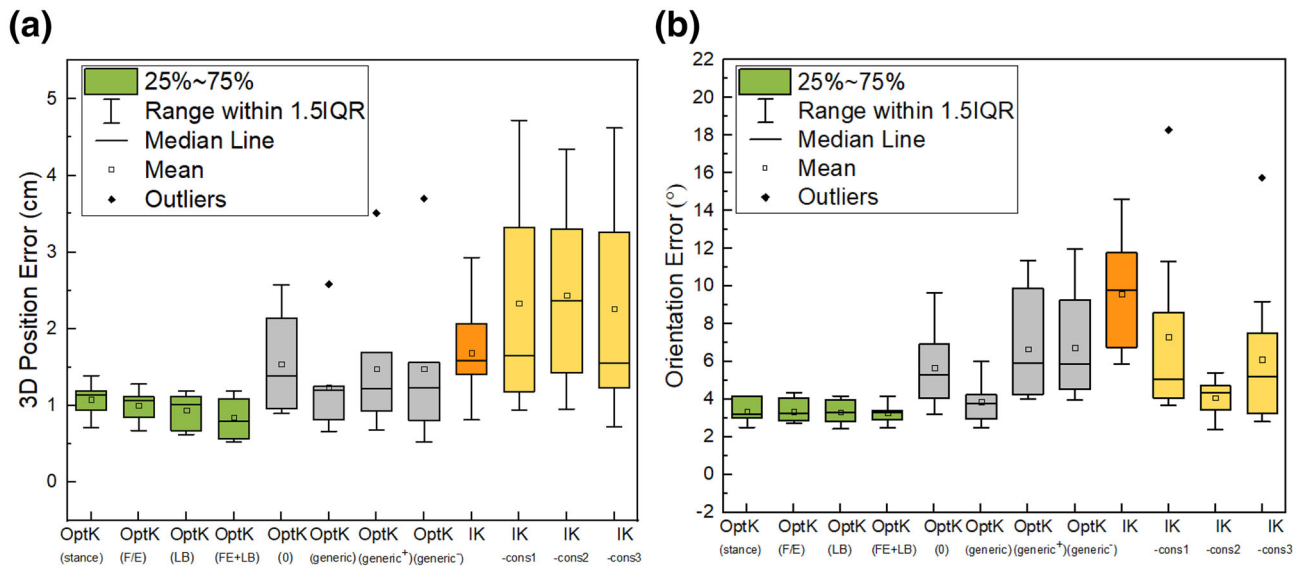


**FIGURE 3.** The mean absolute error of spine alignments of the ten subjects between different kinematic solutions and X-rays in vertebral body center in terms of (a) 3-dimensional position (T1-L5) and (b) sagittal orientation angle (T7-L5). Joint angles in the upper thoracic spine (T1-T7) were not compared due to the relative low quality of the bone geometry on X-ray. Also for healthy subjects the relative joint orientations on frontal plane of stance were too small to be excluded, as it might be too sensitive to measurement errors. Abbreviations are referred to Fig. 2. OptK<sub>PE = generic</sub><sup>+</sup> and OptK<sub>PE = generic</sub> refer to OptK solutions using upper and lower limit of the generic stiffness. IK-cons1 refers to the solutions using Christophy *et al.*,<sup>3</sup> IK-cons2 refers to the solutions using Bruno *et al.*,<sup>2</sup> IK-cons3 refers to the solutions using Shojaei *et al.*,<sup>23</sup>.

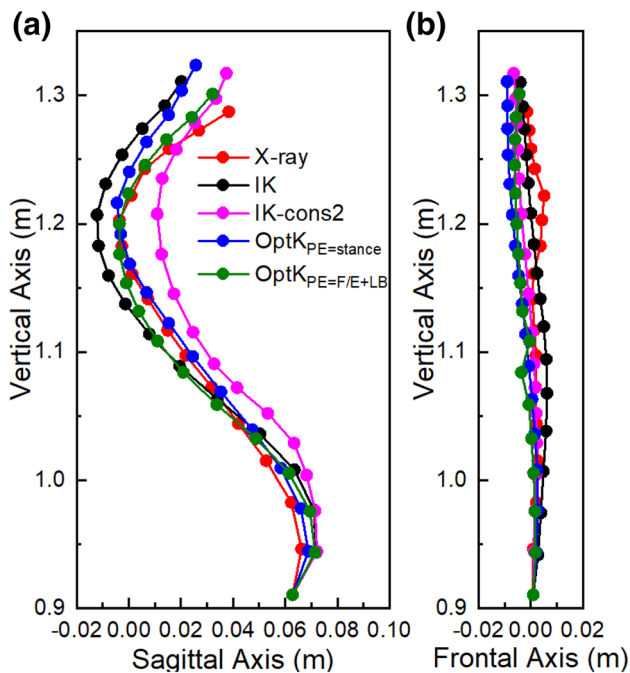


**FIGURE 4.** Representative examples of the spine alignments from different kinematic solutions and X-rays for one subject, shown as the positions of the center of vertebral body from T1 (top) to L5 (bottom) in the sagittal plane (a) and in the frontal plane (b). Abbreviations are referred to Fig. 2. Note that not all kinematic solutions are presented to save the clarity of the figure given the similarities of the predicted spine alignments of the other optimization methods, and here IK-cons2 refers to the solutions obtained using Bruno *et al.*,<sup>2</sup>.

previous *in vitro* loading-displacements tests mainly focus on their neutral zones (over which a vertebra moves with minimal resistance<sup>24</sup>) and physiological ranges of motion under applied maximal external moments (high-resistance zone). Therefore, we calculated the *F/E* and *LB* bending stiffness values for all thoracolumbar levels at the neutral zones and high-resistance zones, corresponding to passive moments 0.1 Nm (assuming the vertebra were under minimal internal resistance against bending) and high moments respectively. The high moments were determined based on the calculated main *F/E* and *LB* bending moments (see Supplementary material).

As the proposed optimization workflow imposes additional constraints to enforce dynamic consistency as well as effects of mechanical properties, we evaluated to what extent the marker position errors between measured and simulated markers increased compared to IK where least-square minimization at each time frame was used. Therefore, the root mean square difference between measured and simulated marker positions was calculated (averaged over all frames of the motions) for the six approaches and compared that with IK.

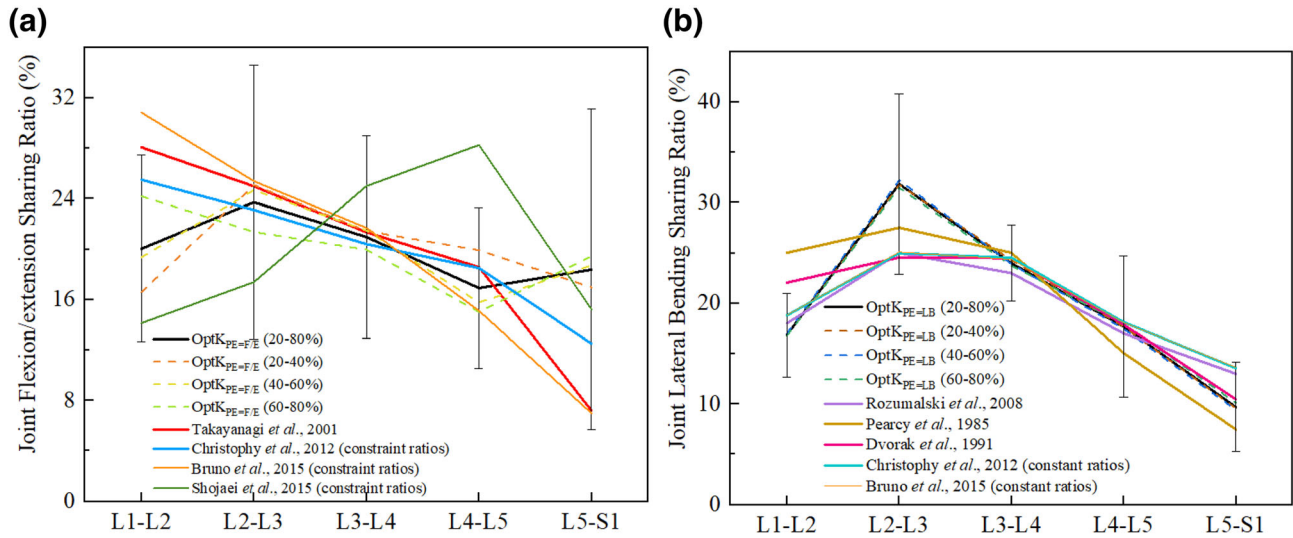


**FIGURE 5.** The motion sharing ratio (MSR) of lumbar intervertebral joints during flexion/extension (F/E) and lateral bending (LB) over time, including the average MSR pattern of all subjects (error bars shown as their standard deviations) between the 20 and 80th percentile and also between smaller divided percentiles: 20–40th percentile, 40–60th percentile, and 60–80th percentile. Abbreviations are given in Fig. 2.

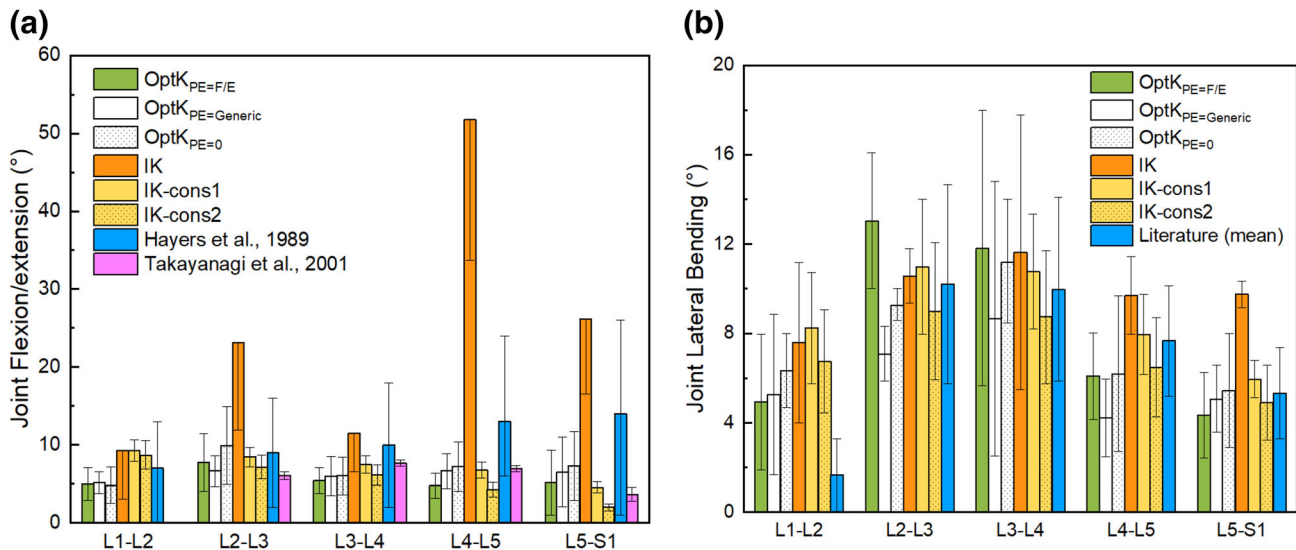


**FIGURE 6.** The range of motion for the lumbar intervertebral joints in: (a) flexion/extension and (b) lateral bending. The model estimations were compared to *in vivo* measurements, where for flexion/extension the references measured similar maximal flexion in a seated pose while for lateral bending the reference data are averaged from literature by Rozumalski *et al.*,<sup>21</sup> Percy *et al.*,<sup>19</sup> Dvorak *et al.*,<sup>5</sup> and Li *et al.*<sup>12</sup> The error bars indicate the standard deviation of the data among the subjects. Note for brevity, only lower standard deviations for IK solutions are shown. IK-cons1 refers to the solutions using Christophy *et al.*,<sup>3</sup> IK-cons2 refers to the solutions using Bruno *et al.*,<sup>2</sup>. As IK-cons3 by Shojaei *et al.*,<sup>23</sup> generated abnormally large joint rotations (over 100°), they were not shown in these figures.

**RESULTS**

Figure 3 shows the boxplots of the mean absolute errors of the spine alignments derived from different kinematic solutions compared to X-rays. Figure 4 shows representative spine alignment curves of one subject. Among the different approaches, the spine

alignment calculated by the Opt-program with calibrated PE were closer to the curve on X-ray than IK and IK-cons solutions. The average errors of these OptK solutions over all subjects varied between 8.5 to 10.1 mm in CoG positions and between 3.29° and 3.38° in sagittal joint orientation angles. In contrast, for IK

and IK-cons solutions, the average errors over all subjects were much larger, with a range of 15.2 and 24.3 mm respectively in CoG distances and a range of 4.04° and 6.08° respectively in joint orientation angles. In addition, differences were found among the alignment solutions of the Opt-program (Fig. 3). The OptK<sub>PE = F/E + LB</sub> solution (with PE calibrated from optimizing the combined motion of *F/E* and LB) showed best agreement in both CoG positions and joint orientations with X-ray (error = 8.5 mm, 3.29°, respectively), but OptK<sub>PE = 0</sub> solution (without PE forces) and OptK<sub>PE = generic</sub> solution (using generic PE parameters) showed least agreement (error = 15.4 mm, 5.68°) and the second least agreement (error = 12.1 mm, 3.50°), respectively. The errors of joint orientations by level are additionally presented in supplementary materials.

Each participant demonstrated a unique pattern of lumbar MSR. The CMC values of all the lumbar MSRs of the overall 20–80th percentile were 0.41 for *F/E* and 0.84 for LB, indicating that the similarity between subjects was low, especially for *F/E*. Figure 5 shows the average MSR pattern of all subjects (SD were shown as error bars) between the 20–80th percentile and also between smaller divided percentiles of the motion cycle: 20–40th percentile, 40–60th percentile and 60–80th percentile. In terms of the overall 20–80th percentile, the values of the MSRs and the overall decreasing pattern for *F/E* and LB from L1 to L5 were similar to *in vivo* studies<sup>5,19,21,25</sup> and the constraints ratios by Christophy<sup>3</sup> and Bruno.<sup>2</sup> For LB, the largest ratios were seen at joint L2-L3 for all studies. The MSR patterns among the three small divided percentiles of the motion cycle were diverse for *F/E*, especially in L1-L2 and L5-S1, whereas a much closer agreement was found for LB.

The average lumbar intervertebral RoM of all subjects during *F/E* and LB are shown in Fig. 6. The *F/E* RoM estimated with the opt-program were comparable to the literature<sup>9,25</sup> measuring maximal *F/E* while seated using medical images. In contrast, abnormal large RoM were estimated using IK. For LB RoM, all solutions fell within one SD of the average value of four reported Refs.<sup>5,12,19</sup> and<sup>21</sup> except for joint L1-L2. For the thoracic spine, the *F/E* ROM using the OptK were in a reasonable range (less than 3.15°), which was consistent with the fact as the subjects were required to keep an upright thoracic spine during *F/E* movement. However, for IK solutions, the estimated *F/E* RoM were in a large and unrealistic range (9.38° and 63.42°). In addition, the average range of axial translations of each lumbar intervertebrae during *F/E* were from 5 mm to 12 mm, which is similar to the *in vivo* measurements (4 mm to 9 mm) by Ref. 16.

When optimizing the bending motion, mainly the PE parameters *A* and *B* (Eq. (3)) in the main bending directions changed from initial generic values (to a range of 0.4 to 4.57 times) while the parameters in the other rotational directions barely changed. The calibrated *F/E* parameters of OptK<sub>PE = F/E</sub> and LB parameters of OptK<sub>PE = LB</sub> were similar to those of OptK<sub>PE = F/E+LB</sub> respectively. Figure 7 shows the changed values of the *F/E* and LB stiffness of the solution OptK<sub>PE = FE+LB</sub>. In general, the stiffness values in low-resistance zone (neutral zone) tended to be smaller than generic stiffness, with the stiffness values of most intervertebral levels being below the lower bound of the nominal range. However, in the high-stiffness zone, a large number of the stiffness values changed to be greater than those in the low-stiffness zone. Most subjects showed stiffer values compared to the generic ones.

The average root mean square errors between estimated and measured marker positions during dynamic bending motions over all subjects were 4.8 mm and 7.7 mm for all the IK and OptK solutions respectively, with both solutions staying well below the error limit of 20.0 mm recommended by OpenSim. The computation time for a simulation of dynamic motion with 100 interval points varied between 2100s and 9210s. Rigid body assumption<sup>27</sup> for the marker cluster was evaluated and—with variability of inter-marker distances being 0.27 mm ( $\pm 0.04$ ) mm and relative variability being 0.58% ( $\pm 0.1\%$ )- confirmed.

## DISCUSSION

The proposed dynamic optimization framework aimed to solve spine kinematics based on 3D skin-marker positions while simultaneously calibrating spine stiffness. Previously used methods and models for solving spine kinematics are commonly static-based and are constrained with strict kinematics bounds. Our proposed optimization approach enforces dynamic consistency in the entire skeletal system and over the entire time-trajectories, as well as the subject-specific nonlinear properties of joint stiffness. Thereby the approach prevents unrealistic joint motions and kinematic inconsistencies caused by uncertainties in body segment parameters and experimental measurement errors.

Our method estimated spinal alignment in stance from measured skin markers and compared this with spinal alignment measured using X-rays-based methods. The estimates using the developed optimization-based approach were better than the solutions of the state-of-the-art IK and IK with constraints methods. In addition, the averaged FE and LB MSRs matched



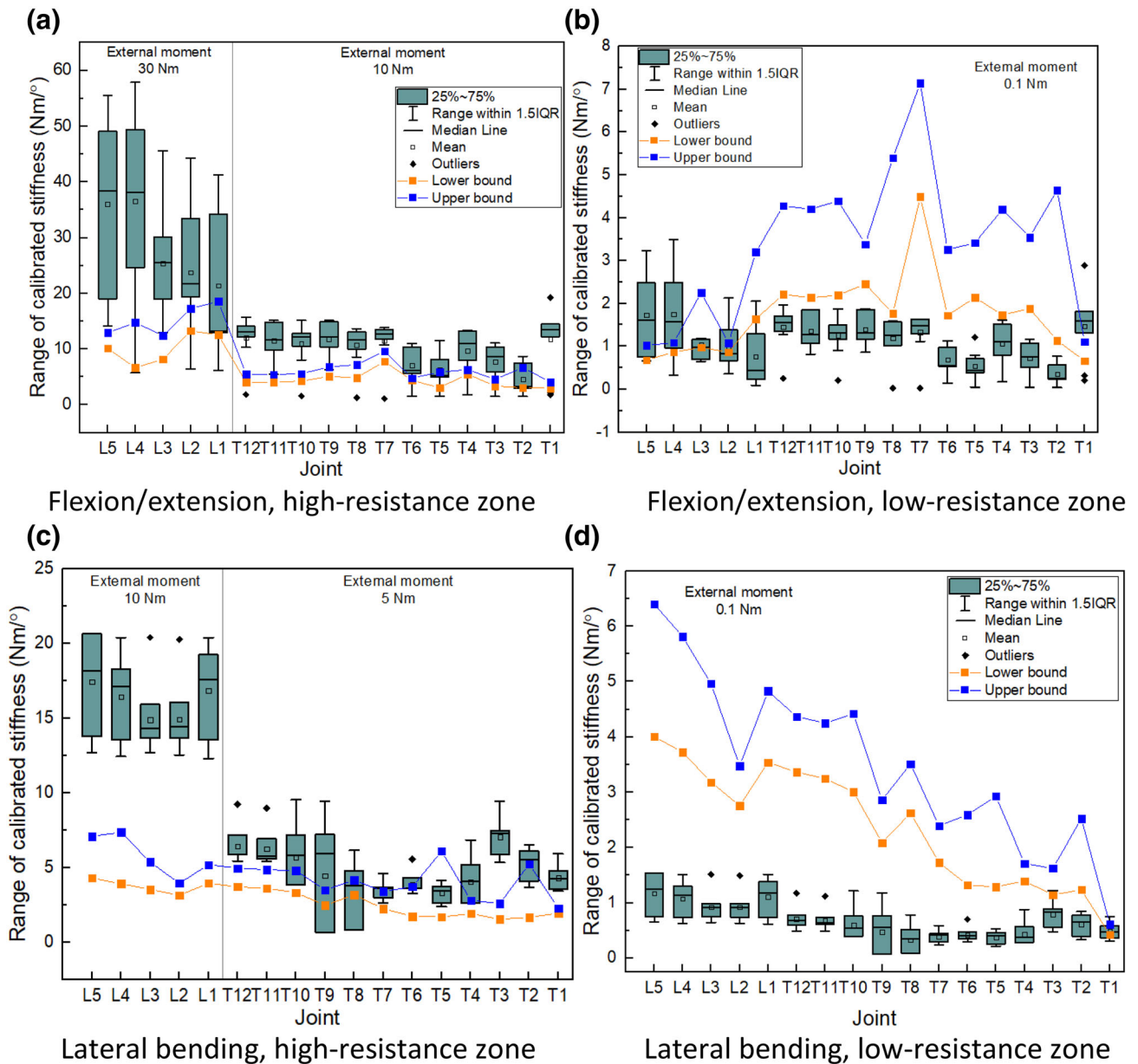


**FIGURE 7.** The calibrated stiffness values in the directions of flexion/extension and lateral bending from T1-T2 to L5-S1. The upper and lower bounds refer to the nominal range of generic stiffness in Ref. 26, considering stiffening effect of compressive follower load. External moments in the high-resistance zone were based on the main bending moments of the thoracolumbar spine in the optimized kinematic solutions (see Supplementary Fig. 2).

the reported overall pattern, *in vivo* values reported in literature as well as the constraint ratios by Christophy<sup>3</sup> and Bruno.<sup>2</sup> Compared to the abnormal high RoM in the unconstrained IK solutions, both the estimated lumbar and thoracic joint rotations fell within a reasonable and acceptable range when using the OptK solutions. The similarities between our estimations using the developed optimization-based method and published results indicate that the estimations were in good agreement with the general physiological pattern of spine movement, with our

method outperforming standard IK methods when solving the spine kinematics redundancy problem.

Interestingly, our optimization method provides the possibility to account for subject-specific variance in spine stiffness when solving the kinematics distribution problem. Using this approach, we found diverse MSR pattern of the lumbar spine across all the subjects, especially for *F/E*, with MSR pattern changing during the spine *F/E* movement. This confirms large movement pattern variations among individuals during the movement cycle, as for example reported in the video

fluoroscopy study by Breen *et al.*<sup>1</sup> Furthermore, the model with generic kinematic constraints estimated reasonable lumbar joint RoM, but failed to capture the subject-specific kinematic pattern, as reflected by the large errors between estimated and X-rays-based vertebral body CoG positions (24.3 mm) and joint orientations (6.08°) calculated using the IK-cons solutions. Due to the nature of changing kinematic relationships across spinal segments, the generic joint kinematic constraints might be capable of representing generic motion pattern of a group of measured population but not be sufficient to account for subject- and movement-specific variation in spinal kinematic coupling. This suggests that the proposed optimization approach was more optimal than IK with generic kinematic constraints methods.

In addition, the proposed method enables accounting for nonlinear passive element (PE) contributions to the spinal dynamic equilibrium on a subject-specific basis through subject-specific tuning based on an individual's dynamic motion pattern. As a result, the OptK solutions with calibrated PE showed better estimation of the spine alignment than the solutions without PE contributions and the solutions using different sets of the generic PE values (i.e., no calibration). Therefore, the results indicate that the subject-specific calibration of stiffness facilitates the reduced errors rather than higher or lower stiffness values. Solely using the optimization approach without PE contribution or calibration accounts for dynamic consistency, which helps estimate more smooth movement compared to IK and IK-cons. It however does not increase estimation accuracy compared to OptK solutions that account for PE contributions. Furthermore, increasing the amount of subject-specific information on spinal alignment by calibrating PE for the combined *F/E* and LB motion (OptK<sub>PE = F/E + LB</sub>) showed the best agreement with alignment on X-ray, as the dynamic bending motion contains more information to provide valid (i.e., representative of the subjects) parameter estimates.<sup>7</sup> Therefore, the increased accuracy in estimating spine alignment was related to the inclusion of PE contribution, the calibration of PE properties, and the amount of subject-specific information of spine motions.

Methods that non-invasively determine *in vivo* stiffness of individual functional spinal units are lacking. Nonetheless, we indirectly evaluated the effect of parameter calibration by comparing the calibrated stiffness values to a range of generic stiffness values<sup>26</sup> and previously reported stiffness patterns in subjects with similar age as our test subjects. After parameter calibration, for most subjects spinal stiffness in the low-resistance zone (neutral zone) decreased, but spinal stiffness in the high-resistance zone increased.

This phenomenon is consistent with studies on aging or spine pathology,<sup>15</sup> where the reduced joint mobility but increased size of the neutral zone was related to aging or disc degeneration, thereby being regarded as an indicator of clinical instability. Meanwhile, increased spinal stiffness and reduced flexibility in *F/E* and LB were observed in studies (e.g., Refs. 11 and 15) that assessed the mobility of degenerated spines. Although the subjects in this study were not considered as pathological subjects, natural spine aging can be expected especially given their age range. Therefore, we believe the PE parameter calibration was reasonable and in agreement with physiological conditions of the subjects. Moreover, the improved accuracy of kinematic estimations when using calibrated PE yields another indirect confirmation of the effectiveness of the developed optimization-based approach.

It should be stressed that the joint kinematics are optimized based on input kinematic information of truly measured marker positions. Therefore, the (relatively rough) maximal range of motion of the spine segment is known to a certain extent, and this can reflect the corresponding trunk mobility and therefore the joint stiffness. Although our indirect validation demonstrates that calibrating parameters improved the estimation of joint kinematics, it is likely that more accurate stiffness parameters can be obtained when using extended input data. For example, using 'true' kinematic data based on sophisticated measures such as 3D video fluoroscopy, as they can present the positions of vertebra during a continuous motion with high accuracy. In this case, the proposed optimization approach can solely calibrate stiffness without optimizing joint kinematics. Such independent calibration evaluation approach offers an avenue for further research.

Nevertheless, when using the OptK solutions, the *F/E* and L/B RoM of specific lumbar joints were slightly smaller than the mean *in vivo* values reported in literature. This could be caused by specimen variance, e.g., age and specimen physical conditions. For example, our subjects are much older than those in the referred studies (mean age around 27 to 40 years). In addition, the measured RoM could also be related to the test pose. Since for our measurements, the subjects were instructed to perform *F/E* and LB in a seated pose, and with their hands crossing behind their head during *F/E*. A review<sup>28</sup> suggested that compared to free standing pose, reduced spinal RoM caused by constrained poses were seen in previous *in vivo* studies. The added values of imposing additional dynamic constraints and effects of mechanical properties (OptK solutions) did indeed result in slightly higher average differences between estimated and measured marker positions than IK solutions, the root mean square errors for all OptK

solution were all within the recommended limit by OpenSim.

Limitations should be taken into account when interpreting the results. It should be noted that the measurement precision and skin movement artefacts could also affect the simulation accuracy. We used some custom-designed lightweight 3D-clusters (the cluster shape has been validated in Ref. 17). Our method implicitly accounts for potential skin artefacts and palpation errors by allowing a moderate deviation of the simulated marker coordinates with respect to measurement. Explicitly introducing additional constraints based on more sophisticated measures can be helpful to further enhance the accuracy of marker-based simulation. For example, Ma *et al.*,<sup>13</sup> proposed a Bayesian prediction model that accounted for soft tissue errors by introducing boundary conditions of the initial and final spatial relationships between the vertebrae and sensors defined by the radiographic images, resulting in a mean error of intervertebral joint angles being 1.45°. Overbergh *et al.*,<sup>18</sup> and Severijns *et al.*,<sup>22</sup> who used the same spinal marker placement protocol as us aimed to further reduce palpation errors by correcting marker position based on extra information from radiography (see Supplementary material). Future research aiming to improve the estimation effect might benefit from comparing kinematic solutions generated by different marker protocols to the ‘gold standard’ data of vertebra positions, collected using more sophisticated measures such as 3D video fluoroscopy, in order to determine the marker placement protocol with the least tracking errors.

In conclusion, we proposed a force-dependent dynamic optimization approach for solving spine kinematics and calibrating subject-specific mechanical properties. Marker-based estimations of spine kinematics were improved by accounting for the dynamic consistency of spinal movement. The ability to account for subject-specific stiffness measured non-invasively during dynamic motions drastically improved the current estimations of spinal alignment of the control subjects but may become even more relevant when studying subjects with adult spinal deformity. As such, this work is at the basis of enhanced insights into spinal mechanics through more physiologically-accurate biomechanical simulations in health and disease. Script of the proposed approach will be available upon acceptance in the online OpenSim repository (simtk.org).

## SUPPLEMENTARY INFORMATION

The online version contains supplementary material available at <https://doi.org/10.1007/s10439-021-02774-3>.

## ACKNOWLEDGEMENTS

The authors would like to acknowledge the financial support from National Key Research and Development Program of China (No. 2019YFB1312501), China Scholarship Council (award to the first author, CSC No. 201706230047), Research Foundation Flanders (FWO) under PhD grants (No. 1S35416N and No. SB/1S56017N), the “Medtronic educational chair for spinal deformity research”, internal UZ Leuven Academic research funding (KOOR), and the KU Leuven Internal Funds (Grant No. C24/17/095—ASESP-P).

## CONFLICT OF INTEREST

We have no conflicts of interest to disclose. No benefits in any form have been or will be received from a commercial party related directly or indirectly to the subject of this manuscript.

## REFERENCES

- <sup>1</sup>Breen, A., and A. Breen. Uneven intervertebral motion sharing is related to disc degeneration and is greater in patients with chronic, non-specific low back pain: an in vivo, cross-sectional cohort comparison of intervertebral dynamics using quantitative fluoroscopy. *Eur. Spine J.* 27:145–153, 2018.
- <sup>2</sup>Bruno, A. G., M. L. Bouxsein, and D. E. Anderson. Development and validation of a musculoskeletal model of the fully articulated thoracolumbar spine and Rib cage. *J. Biomech. Eng.* 137:2015.
- <sup>3</sup>Christophy, M., N. A. Faruk Senan, J. C. Lotz, and O. M. O’Reilly. A musculoskeletal model for the lumbar spine. *Biomech. Model Mechanobiol.* 11:19–34, 2012.
- <sup>4</sup>De Groote, F., A. L. Kinney, A. V. Rao, and B. J. Fregly. Evaluation of direct collocation optimal control problem formulations for solving the muscle redundancy problem. *Ann. Biomed. Eng.* 44:2922–2936, 2016.
- <sup>5</sup>Dvorak, J., M. M. Panjabi, J. E. Novotny, D. G. Chang, and D. Grob. Clinical validation of functional flexion-ex-

- tension roentgenograms of the lumbar spine. *Spine* 16:943–950, 1991.
- <sup>6</sup>Eskandari, A. H., N. Arjmand, A. Shirazi-Adl, and F. Farahmand. Hypersensitivity of trunk biomechanical model predictions to errors in image-based kinematics when using fully displacement-control techniques. *J. Biomech.* 84:161–171, 2019.
  - <sup>7</sup>Falisse, A., S. V. Rossom, I. Jonkers, and F. De Groote. EMG-driven optimal estimation of subject-SPECIFIC hill model muscle-tendon parameters of the knee joint actuators. *IEEE Trans. Biomed. Eng.* 64:2253–2262, 2017.
  - <sup>8</sup>Falisse, A., G. Serranoli, C. L. Dembia, J. Gillis, I. Jonkers, and F. De Groote. Rapid predictive simulations with complex musculoskeletal models suggest that diverse healthy and pathological human gaits can emerge from similar control strategies. *J. R. Soc. Interface* 16:20190402, 2019.
  - <sup>9</sup>Hayes, M. A., T. C. Howard, C. R. Gruel, and J. A. Kopta. Roentgenographic evaluation of lumbar spine flexion-extension in asymptomatic individuals. *Spine* 14:327–331, 1989.
  - <sup>10</sup>Ignasiak, D., S. Dendorfer, and S. J. Ferguson. Thoracolumbar spine model with articulated ribcage for the prediction of dynamic spinal loading. *J. Biomech.* 49:959–966, 2016.
  - <sup>11</sup>Kettler, A., F. Rohlmann, C. Ring, C. Mack, and H. J. Wilke. Do early stages of lumbar intervertebral disc degeneration really cause instability? Evaluation of an in vitro database. *Eur. Spine J.* 20:578–584, 2011.
  - <sup>12</sup>Li, G., S. Wang, P. Passias, Q. Xia, G. Li, and K. Wood. Segmental in vivo vertebral motion during functional human lumbar spine activities. *Eur. Spine J.* 18:1013–1021, 2009.
  - <sup>13</sup>Ma, H. T., Z. Yang, J. F. Griffith, P. C. Leung, and R. Y. Lee. A new method for determining lumbar spine motion using Bayesian belief network. *Med. Biol. Eng. Comput.* 46:333–340, 2008.
  - <sup>14</sup>Marra, M. A., V. Vanheule, R. Fluit, B. H. Koopman, J. Rasmussen, N. Verdonshot, and M. S. Andersen. A subject-specific musculoskeletal modeling framework to predict in vivo mechanics of total knee arthroplasty. *J. Biomech. Eng.* 137:2015.
  - <sup>15</sup>Mimura, M., M. M. Panjabi, T. R. Oxland, J. J. Crisco, I. Yamamoto, and A. Vasavada. Disc degeneration affects the multidirectional flexibility of the lumbar spine. *Spine* 19:1371–1380, 1994.
  - <sup>16</sup>Nagel, T. M., J. L. Zitnay, V. H. Barocas, and D. J. Nuckley. Quantification of continuous in vivo flexion-extension kinematics and intervertebral strains. *Eur. Spine J.* 23:754–761, 2014.
  - <sup>17</sup>Needham, R., R. Naemi, A. Healy, and N. Chockalingam. Multi-segment kinematic model to assess three-dimensional movement of the spine and back during gait. *Prosthet. Orthot. Int.* 40:624–635, 2016.
  - <sup>18</sup>Overbergh, T., P. Severijns, E. Beaucage-Gauvreau, I. Jonkers, L. Moke, and L. Scheys. Development and validation of a modeling workflow for the generation of image-based, subject-specific thoracolumbar models of spinal deformity. *J. Biomech.* 110:2020.
  - <sup>19</sup>Pearcy, M., and J. Shepherd. Is there instability in spondylolisthesis? *Spine* 10:175–177, 1985.
  - <sup>20</sup>Petit, Y., C. É. Aubin, and H. Labelle. Patient-specific mechanical properties of a flexible multi-body model of the scoliotic spine. *Med. Biol. Eng. Comput.* 42:55–60, 2004.
  - <sup>21</sup>Rozumalski, A., M. H. Schwartz, R. Werve, A. Swanson, D. C. Dykes, and T. Novacheck. The in vivo three-dimensional motion of the human lumbar spine during gait. *Gait Posture* 28:378–384, 2008.
  - <sup>22</sup>Severijns, P., T. Overbergh, A. Thauvoeye, J. Baudewijns, D. Monari, L. Moke, K. Desloovere, and L. Scheys. A subject-specific method to measure dynamic spinal alignment in adult spinal deformity. *Spine J.* 20:934–946, 2020.
  - <sup>23</sup>Shojaei, I., N. Arjmand, J. R. Meakin, and B. Bazrgari. A model-based approach for estimation of changes in lumbar segmental kinematics associated with alterations in trunk muscle forces. *J. Biomech.* 70:82–87, 2018.
  - <sup>24</sup>Smit, T. H., M. S. van Tunen, A. J. van der Veen, I. Kingma, and J. H. van Dieen. Quantifying intervertebral disc mechanics: a new definition of the neutral zone. *BMC Musculoskelet. Disord.* 12:38, 2011.
  - <sup>25</sup>Takayanagi, K., K. Takahashi, M. Yamagata, H. Moriya, H. Kitahara, and T. Tamaki. Using cineradiography for continuous dynamic-motion analysis of the lumbar spine. *Spine* 26:1858–1865, 2001.
  - <sup>26</sup>Wang, W., D. M. Wang, F. De Groote, L. Scheys, and I. Jonkers. Implementation of physiological functional spinal units in a rigid-body model of the thoracolumbar spine. *J. Biomech.* 98:2019.
  - <sup>27</sup>Wang, W., D. M. Wang, M. Wesseling, B. Xue, and F. Y. Li. Comparison of modelling and tracking methods for analysing elbow and forearm kinematics. *Proc. Inst. Mech. Eng. Part H* 233(11):1113–1121, 2019.
  - <sup>28</sup>Widmer, J., P. Fornaciari, M. Senteler, T. Roth, J. G. Snedeker, and M. Farshad. Kinematics of the spine under healthy and degenerative conditions: a systematic review. *Ann. Biomed. Eng.* 47:1491–1522, 2019.
  - <sup>29</sup>Wilke, H. J., A. Herkommer, K. Werner, and C. Liebsch. In vitro analysis of the segmental flexibility of the thoracic spine. *PLoS ONE* 12:2017.
  - <sup>30</sup>Zemp, R., R. List, T. Gulay, J. P. Elsig, J. Naxera, W. R. Taylor, and S. Lorenzetti. Soft tissue artefacts of the human back: comparison of the sagittal curvature of the spine measured using skin markers and an open upright MRI. *PLoS ONE* 9:2014.

**Publisher's Note** Springer Nature remains neutral with regard to jurisdictional claims in published maps and institutional affiliations.